Catalysis Letters (2020) 150:1418–1426
https://doi.org/10.1007/s10562-019-03033-w

# Cooperation Between Active Metal and Basic Support in Ni-Based Catalyst for Low-Temperature $CO_2$ Methanation

**Yuan Ma[1] · Jiao Liu[2] · Mo Chu[1] · Junrong Yue[2] · Yanbin Cui[2] · Guangwen Xu[3]**

Received: 7 September 2019 / Accepted: 31 October 2019 / Published online: 13 November 2019
© Springer Science+Business Media, LLC, part of Springer Nature 2019

## Abstract

The key challenge for $CO_2$ methanation, an eight-electron process under kinetic limitation, relies on the design of non-noble metal catalysts so as to achieve high activity at low reaction temperatures. In this work, four Ni-based catalysts with different supports were prepared and tested for $CO_2$ methanation at 250–550 °C in a fixed bed quartz reactor and further characterized to reveal the structure–function relationship. The Ni-based catalysts followed an activity order of $Ni/CeO_2 > Ni/Al_2O_3 > Ni/TiO_2 > Ni/ZrO_2$, especially at temperatures lower than 350 °C. $H_2$-TPR and TPD results indicated that the interaction between nickel and support was strong and the metallic nickel was well dispersed in the $Ni/Al_2O_3$ catalyst, while more amount of $CO_2$ was adsorbed on the weak basic sites in the $Ni/CeO_2$ catalyst. By establishing the correlation between the catalytic performance and the catalyst structure, it was found that the Ni nanoparticles and basic support serve as $H_2$ and $CO_2$ active centers respectively and cooperatively catalyze $CO_2$ methanation, resulting in high low-temperature reaction activity.

### Graphic Abstract

High $CO_2$ conversion was achieved over $Ni/CeO_2$ catalyst at 300 °C for its high $H_2$ uptake on Ni nanoparticles and high $CO_2$ adsorption capacity on the support with weak basic sites and cooperatively to catalyze $CO_2$ methanation.

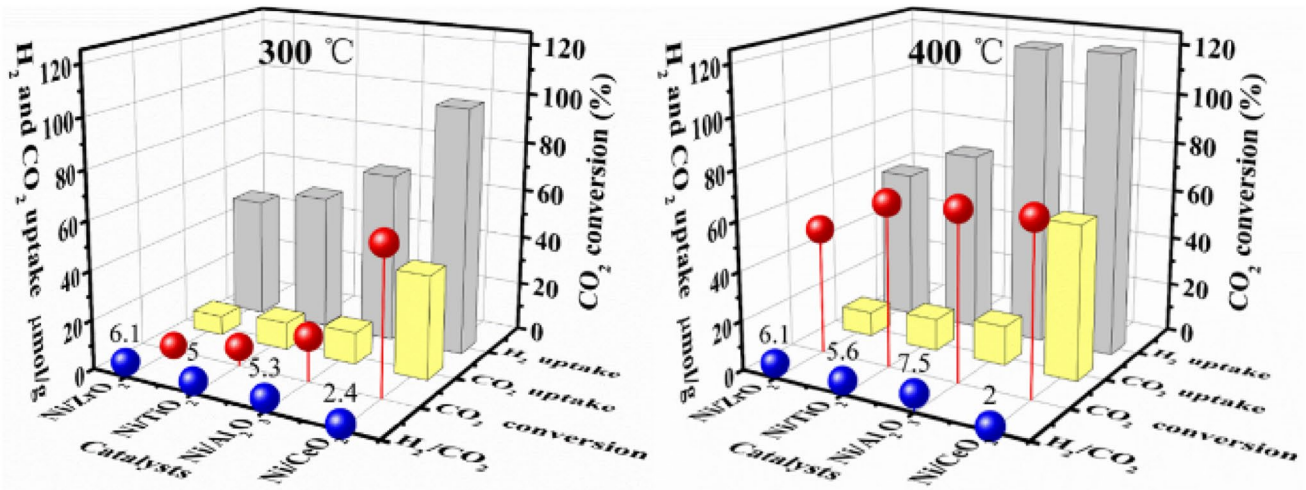


**Keywords** $CO_2$ methanation · $Ni/CeO_2$ · Catalyst · Support · Basic site · TPD

## 1 Introduction

Carbon dioxide as an important component of greenhouse gas and C1 resource has been widely investigated for its capture, storage and utilization [1–3]. $CO_2$ methanation

✉ Jiao Liu
liujiao@ipe.ac.cn

Extended author information available on the last page of the article

(known as Sabatier reaction) which would reduce $CO_2$ emissions and produce natural gas, is considered to be one of the most effective and practical technologies for $CO_2$ recycling [4]. As a volume-reduce and exothermic reaction, $CO_2$ methanation is favored at elevated pressures and low temperatures, whereas kinetic limitation reduces conversion efficiency of $CO_2$ to methane [5].

Noble metals, especially Ru and Rh, are very active and selective for $CO_2$ methanation at low temperatures [6]. Lin et al. [7] investigated the effect of $TiO_2$ structure on the dispersion of Ru nanoparticles and found that the high interaction between $RuO_2$ and rutile-$TiO_2$ promotes the dispersion of active sites and prevent their aggregation. Therefore, Ru/rutile-$TiO_2$ shows high thermal stability and catalytic activity with a $CO_2$ conversion of 65% at 300 °C. Karelovic et al. [8] reported that methane selectivity was 100% over the $Rh/Al_2O_3$ catalyst at temperatures between 185 and 200 °C. However, the turnover frequency (TOF) for $CH_4$ formation was found to be dependent on Rh particle size. Larger Rh particles are up to four times more active than smaller particles at low temperature (135–150 °C), whereas at higher temperatures (200 °C) TOFs are similar for all particle sizes.

Ni-based catalysts have also been widely studied for $CO_2$ methanation due to its low cost and high activity [5, 9–11]. $SiO_2$, MgO, $Al_2O_3$, $TiO_2$, $CeO_2$, $ZrO_2$ and many other oxides have been exploited as supports for Ni catalysts in $CO_2$ methanation [12–14]. Liu et al. [15] prepared a well-dispersed $Ni/TiO_2$ catalyst with small Ni particle size (2.2 nm) and obtained high $CO_2$ conversion (96%) at 260 °C. He et al. [16] reported a Ni–Al hydrotalcite-derived catalyst exhibited narrow Ni particle-size, which reached 82.5% $CO_2$ conversion at 350 °C. Tada et al. [14] studied the effect of various supports ($CeO_2$, α-$Al_2O_3$, $TiO_2$ and MgO) on Ni catalysts for $CO_2$ methanation and found that $Ni/CeO_2$ catalyst showed high $CO_2$ conversion, especially at low temperatures (350 °C).

However, the available results are discordant about how the support affects the activity of $CO_2$ methanation. Vogt et al. [17] reported that $CO_2$ methanation over Ni catalyst is structure-sensitive. The support plays key roles not only in the dispersion of Ni catalysts but also in the promotion of $CO_2$ adsorption, activation and conversion. Aldana et al. [18] examined the $CO_2$ mthanation over Ni-ceria-zirconia catalysts and revealed that the high catalytic activity was attributed to the weak basic sites of support for the adsorption of $CO_2$. Lin et al. [19] found that incorporation of $ZrO_2$ into $Ni/Al_2O_3$ weakened the Ni-$Al_2O_3$ interaction and increased the amount of active metallic sites and oxygen vacancies, obviously improving the lower temperature catalytic activity. Many studies on the improvement of $CO_2$ methanation at low temperature are based on the dispersion of active metals or basic sites of supports [20–22].

Moreover, the reaction mechanism (e.g., the reaction intermediate and route) is highly correlated with the structure of the active sites and basic sites [23–25]. Wu et al. [26] studied $CO_2$ methanation on both 0.5 wt% and 10 wt% $Ni/SiO_2$ catalysts. The results indicated that the reaction pathways depend on the Ni particle size. The m-HCOO intermediate is intricately involved in $CO_2$ hydrogenation over both $Ni/SiO_2$ catalysts, regardless of the Ni loading and particle size. $CO_2$ hydrogenation likely follows a consecutive pathway on the 0.5 wt% $Ni/SiO_2$ catalyst with small Ni particles, forming CO and $CH_4$. However, the low $H_2$ coverage leads to the quick formation of CO from the m-HCOO intermediate. This process led to high selectivity for CO formation on the 0.5 wt% $Ni/SiO_2$ catalyst. When the Ni loading was increased to 10 wt%, the reaction proceeds through the mixed consecutive and parallel pathways and the selectivity switched to favor $CH_4$ formation.

Nevertheless, Beierlein et al. [27] prepared highly loaded Ni-$Al_2O_3$ catalysts and found that $CO_2$ methanation on Ni-$Al_2O_3$ catalysts is a structure-insensitive reaction and the TOF does not depend on metal-support interactions, the metal-support interface or the particle size. The Ni surface area is the sole microscopic property which determines the $CO_2$ conversion. Therefore, the catalysts with the highest Ni surface areas achieve the highest weight time yields.

In this work, four Ni catalysts supported on γ-$Al_2O_3$, $ZrO_2$, $TiO_2$ and $CeO_2$, respectively were prepared and characterized to understand the interrelationship between the structure and catalytic performance for $CO_2$ methanation. The physic-chemical properties of the catalysts were analyzed by BET, XRD, $H_2$-TPR, $H_2$-TPD and $CO_2$-TPD. In particular, the cooperation between active metal and basic support are discussed in depth.

## 2 Experimental

### 2.1 Catalyst Preparation

$CeO_2$ as a support was prepared by precipitation and hydrothermal treatment. The aqueous solution of $Ce(NO_3)_3{\cdot}6H_2O$ and 7 mol/L NaOH were firstly added dropwise into a reaction vessel maintained at 40 °C under continuous mechanical stirring. Then, the suspending liquid was transferred to a Teflon-lined stainless steel autoclave that was in turn heated to 180 °C and maintained for 24 h. The precipitate was collected by filtration with thoroughly washing with distilled water. $CeO_2$ was finally obtained by drying at 60 °C for 10 h and calcined at 500 °C for 4 h.

$ZrO_2$ as a support was synthesized by precipitation. The aqueous solution of $Zr–(NO_3)_4{\cdot}5H_2O$ and 1 mL/L NaOH were firstly added dropwise into a reaction vessel maintained at 60 °C under continuous mechanical stirring. The

rates of adding the solution and precipitant were controlled to keep the reaction mixture for pH 10. The formed precipitate was aged at 60 °C for 10 h and collected by filtration with thoroughly washing using distilled water. $ZrO_2$ was finally obtained by drying at 60 °C for 12 h and calcined at 500 °C for 4 h.

γ-$Al_2O_3$ as a support was prepared by calcination of pseudo boehmite (from Aluminum Corporation of China) at 500 °C for 4 h and $TiO_2$ was purchased from Aladdin Industrial Corporation of China.

Four nickel-based catalysts were prepared by deposition precipitation. The aqueous solution of $Ni(NO_3)_2{\cdot}6H_2O$ and the support were firstly mixed at 60 °C for 2 h. Then, 1 mol/L NaOH was added dropwise until the pH 10. The suspension was further stirred and aged at 60 °C for 10 h. The formed precipitate was aged at 60 °C for another 10 h and collected by filtration with thoroughly washing using distilled water. The catalyst was finally obtained by drying at 60 °C for 12 h and calcined at 500 °C for 4 h. Theoretically, the nickel loading in the catalysts was fixed at 20 wt%.

### 2.2 Catalyst Characterization and Analysis

$N_2$ adsorption–desorption isotherms at − 196 °C were obtained on a Micrometrics ASAP 2020 HD88 analyzer. Before measurement, the samples were degassed under vacuum at 200 °C for 12 h. The crystal structure of the prepared catalysts was analyzed with X-ray power diffractometry (XRD, X'Pert MPD Pro, PANalytical) at its Cu $K_\alpha$ radiation of λ = 0.154 nm. The patterns were recorded with a scan angle range 5–90° at a scanning speed of 8°/min. The Ni loading on the supports was determined by X-ray fluorescence (XRF, AXIOX, PANalytical).

Temperature programmed reduction (TPR) and $H_2$ or $CO_2$ temperature programmed desorption ($H_2$-TPD or $CO_2$-TPD) of the catalysts were carried out in Auto Chem II2920 (Micrometrics) coupling with MS (TILON, US). Prior to $H_2$-TPR tests, 0.1 g of sample was heated from room temperature to 200 °C at 10 °C/min and maintained for 1 h under He flow. After that, the sample was cooled to 50 °C and then heated to 900 °C at 10 °C/min under a binary gas (10 vol. % $H_2$/Ar). For H2-TPD, 0.1 g of oxide catalyst was firstly reduced in situ under $H_2$/Ar flow at 600 °C for 2 h and then cooled to 50 °C and saturated with $H_2$ for 1 h. After removing the physically adsorbed $H_2$ by purging with He, the sample was heated to 900 °C at a ramping rate of 10 °C/min under He flow. The desorbed $H_2$ was detected simultaneously by a thermal conductivity detector (TCD) and MS. $CO_2$-TPD of pre-reduced samples (0.1 g) was performed in flowing He from 50 to 700 °C with a heating rate of 10 °C/min after adsorption of 10 vol% $CO_2$/Ar at 50 °C for 2 h.

### 2.3 Methanation Test

$CO_2$ methanation was carried out in a quartz fixed-bed reactor (I.D. = 16 mm) at atmospheric pressure. Before the reaction, 500 mg of catalyst (75–109 μm) were reduced at 600 °C for 4 h under 10 vol% $H_2/N_2$ stream (50 mL/min). After reduction, the system was cooled down to reaction temperature under $N_2$ flow (50 mL/min), and the mixture gas of $H_2/N_2/CO_2$ with volume ratio of 4/1/1 was introduced into the reactor and the space velocity (*SV*) was 120,000 mL/g/h. The product gas was analyzed with a micro gas chromatography (Micro3000, Agilent) equipped with TCD. The reaction temperature was monitored by a thermocouple near the bottom of the catalyst bed. The flow rates of $H_2$, $N_2$ and $CO_2$ were controlled by mass flow meters, and $N_2$ was used as an internal standard to calculate the volume flow of each component in the product. The $CO_2$ conversion and $CH_4$ selectivity were calculated with the following equations:

$$X_{CO_2}=\frac{f_{in}y_{CO_2,in}-f_{out}y_{CO_2,out}}{f_{in}y_{CO_2,in}}\times 100\% \quad (1)$$

$$S_{CH_4}=\frac{f_{out}y_{CH_4,out}}{f_{in}y_{CO_2,in}-f_{out}y_{CO_2,out}}\times 100\% \quad (2)$$

where the $X_{CO2}$ and $S_{CH4}$ is the $CO_2$ conversion and $CH_4$ selectivity; $f_{in}$ and $f_{out}$ is the molar feed rate of import and export flow in the reactor; $y_{CO2,in}$, $y_{CO2,out}$ and $y_{CH4,out}$ is the volume fraction of import and export of $CO_2$ and $CH_4$ in the reactor.

## 3 Results and Discussion

### 3.1 Catalytic Performance

Figure 1 shows the $CO_2$ conversion and $CH_4$ selectivity for $CO_2$ methanation at different temperatures over the Ni/$Al_2O_3$, Ni/$ZrO_2$, Ni/$TiO_2$ and Ni/$CeO_2$ catalysts, respectively. The experimental $CO_2$ conversion and selectivity to $CH_4$ were also compared with their thermodynamic equilibrium values calculated using the HSC Chemistry that considers reactions of methanation and reverse water–gas-shift (RWGS). Figure 1a exhibits that for the Ni/$Al_2O_3$, Ni/$TiO_2$ and Ni/$CeO_2$ catalysts, the $CO_2$ conversion increased drastically as the temperature increased from 250 to 400 °C, then reached the maximum and decreased gradually with temperature increasing. For the Ni/$ZrO_2$ catalyst, the $CO_2$ conversion increased as the temperature increased from 250 to 550 °C. These results indicate that for the Ni/$Al_2O_3$, Ni/$TiO_2$ and Ni/$CeO_2$ catalysts, the $CO_2$ methanation was subject to

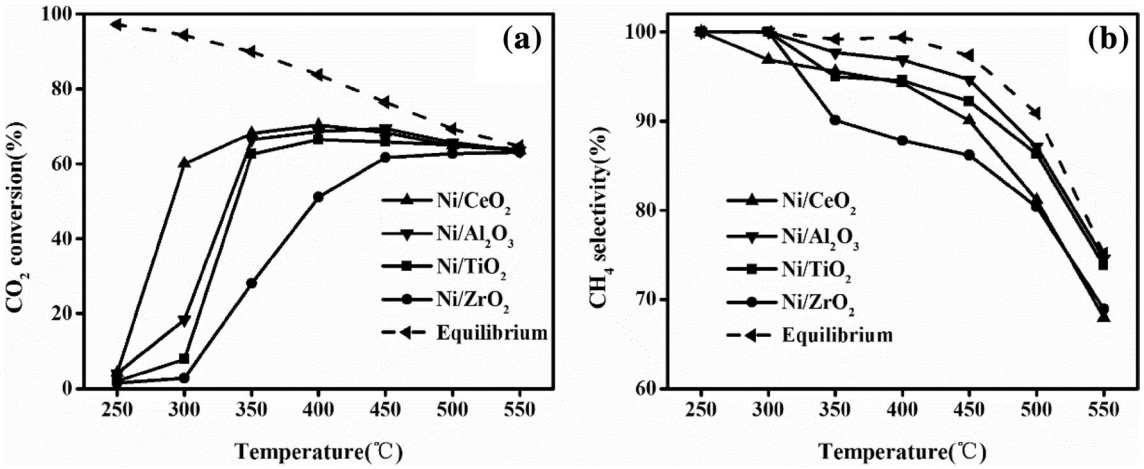


**Fig. 1** **a** $CO_2$ conversion and **b** $CH_4$ selectivity at different temperatures over the Ni-based catalysts with different supports

kinetic control at lower temperatures but to thermodynamics dominance above 400 °C when the equilibrium coefficient becomes smaller at higher temperatures. From Fig. 1b, it can be seen that controlled by the thermodynamics, the selectivity to $CH_4$ decreased with increasing the reaction temperature for all the four catalysts [28, 29].

Moreover, Fig. 1a also demonstrates that the realized $CO_2$ conversion followed an order of $Ni/CeO_2 > Ni/Al_2O_3 > Ni/TiO_2 > Ni/ZrO_2$ and the $Ni/CeO_2$ catalyst showed the highest $CO_2$ conversion at low temperatures, especially at temperatures lower than 350 °C. The $CO_2$ conversion for the $Ni/CeO_2$ catalyst was 60.1% at 300 °C while that for other three catalysts was all lower than 20%.

## 3.2 Catalyst Characterization

The $N_2$ adsorption–desorption isotherms for the four catalysts were all of type IV with a hysteresis loop to characterize the mesoporous structure. The calculated surface area, pore volume and average pore size for the four catalysts are presented in Table 1. The $Ni/Al_2O_3$ catalyst exhibited the highest surface area, and then the $Ni/CeO_2$ and $Ni/ZrO_2$. The $Ni/TiO_2$ catalyst possessed the surface area of only 37 $m^2/g$, and the largest pore volume and pore diameter.

Figure 2 shows the XRD patterns of the calcined (Fig. 2a) and reduced (Fig. 2b) Ni-based catalysts. The NiO diffraction peaks at $2\theta = 37.3°$, 43.3°, and 62.8° corresponding to the (111), (200), and (220) planes of NiO were observed in Fig. 2a. The $NiAl_2O_4$, and $\gamma$-$Al_2O_3$ generally co-presented at $2\theta = 45.9°$ and 66.9° in $Ni/Al_2O_3$ catalyst and overlapped to be difficultly distinguished.

After reduced at 600 °C, the four catalysts all showed the Ni peaks at $2\theta = 44.6°$, 51.9° and 76.5° corresponding to its (111), (200) and (220) planes in Fig. 2b, respectively. This shows that the NiO species were completely reduced

**Table 1** Physic-chemical properties of the Ni-based catalysts with different supports

| Catalyst | BET surface area ($m^2/g$)[a] | Pore volume ($cm^3/g$)[b] | Average pore size (nm)[c] | Ni loading (%)[d] |
|---|---|---|---|---|
| $Ni/Al_2O_3$ | 216 | 0.14 | 7.8 | 18.40 |
| $Ni/CeO_2$ | 77 | 0.13 | 5.6 | 18.75 |
| $Ni/ZrO_2$ | 58 | 0.14 | 6.1 | 17.45 |
| $Ni/TiO_2$ | 37 | 0.25 | 26.5 | 17.38 |

[a]Calculated with BET equation

[b]Referring to the BJH desorption pore volume

[c]Referring to the BJH desorption average pore size (4 × total pore volume/surface area)

[d]Determined by XRF measurement

for these catalysts. Meanwhile, the intensity of the Ni peaks for $Ni/Al_2O_3$ and $Ni/CeO_2$ catalysts are much weaker, which reveals that active sites were well dispersed on $Al_2O_3$ and $CeO_2$ support. The crystal sizes of metallic Ni calculated using the Scherrer equation for the (200) plane were 6.8, 8.2, 21.9 and 33.5 nm for $Ni/Al_2O_3$, $Ni/CeO_2$, $Ni/TiO_2$ and $Ni/ZrO_2$, respectively.

The $H_2$-TPR measurements were carried out to clarify the interaction between nickel species and support. Figure 3a shows the TPR profiles of Ni-based catalysts on different supports. The $Ni/Al_2O_3$, $Ni/TiO_2$ and $Ni/ZrO_2$ catalysts exhibited only one reduction band and the peak temperature followed an order of $Ni/ZrO_2 < Ni/TiO_2 < Ni/Al_2O_3$ indicating the highly dispersed Ni particles and stronger interaction between NiO and $Al_2O_3$ in $Ni/Al_2O_3$ catalyst. For $Ni/CeO_2$ catalyst, three reduction peaks were observed. The first peak at around 248 °C belonged to the reduction of bulk NiO species. The second peak at 355 °C was attributed to the reduction of NiO species which interacted with

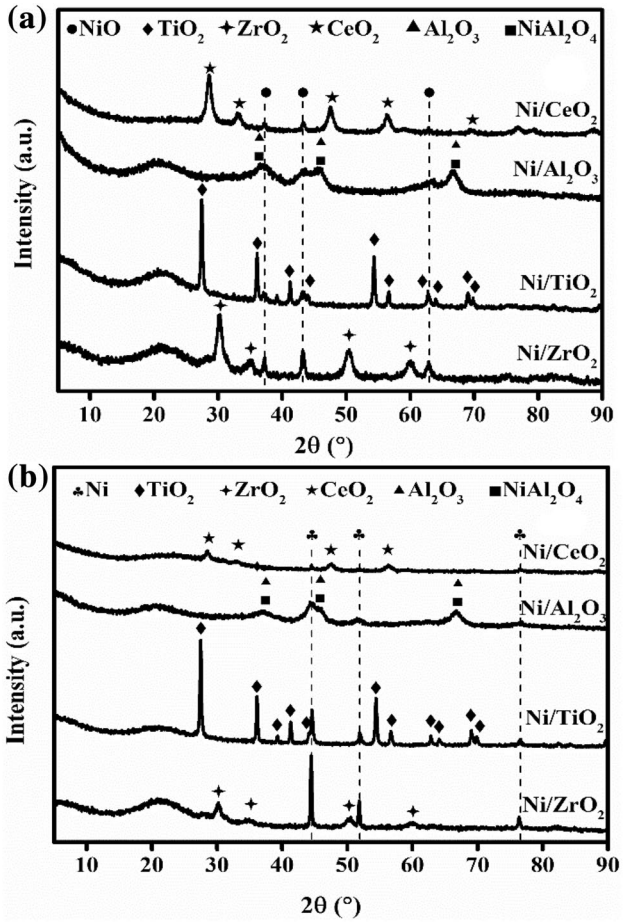


**Fig. 2** XRD patterns of **a** calcined and **b** reduced Ni-based catalysts with different supports

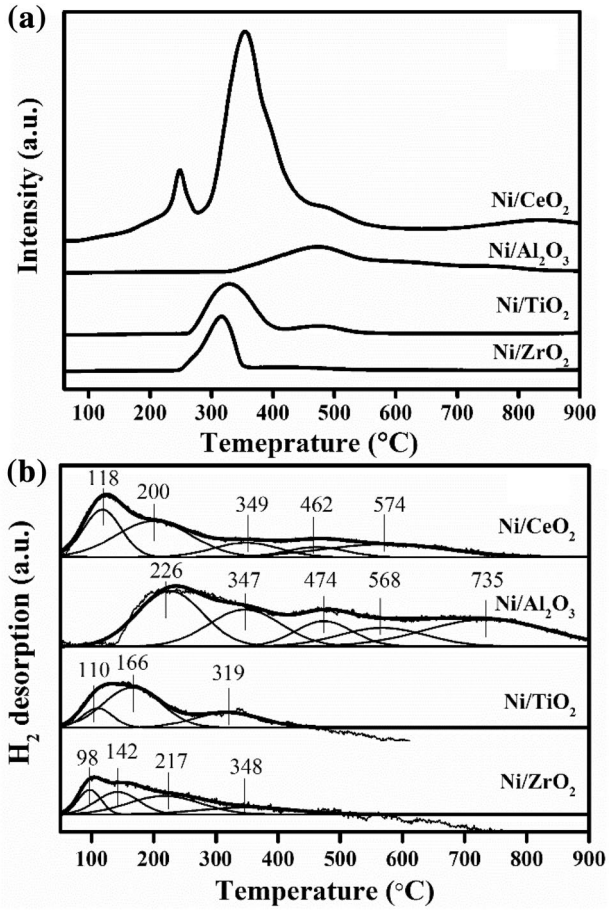


**Fig. 3** **a** $H_2$-TPR and **b** $H_2$-TPD profiles of the Ni-based catalysts with different supports

the support. Finally, the reduction peak around 832 °C was basically identical to the reduction of the $CeO_2$ support [30, 31]. Before methanation tests, the four catalyst were pre-reduced at 600 °C for 4 h under 10 vol% $H_2/N_2$ stream, so the NiO species in these catalysts were all completely reduced to metallic nickel in accordance with the result of XRD in Fig. 2b.

The $H_2$ chemsorption properties of catalysts depending on nickel amount and dispersion were measured by $H_2$-TPD. The irregular shapes in Fig. 3b for all the catalysts could be a consequence of partial overlapping of $H_2$ desorption peaks from the metals with distinct diameters [32], surfaces [33] or positions [34]. Gaussian multi-peak fitting results show that there are several peaks at lower temperatures (< 400 °C) for all the four catalysts. These peaks can be assigned to desorption of $H_2$ that is weakly chemisorbed on the surface with highly dispersed Ni and a high density of defects which could act as traps during surface hydrogen diffusion and thus reduce the activation energy of $H_2$ dissociation. Meanwhile, the higher-temperature (> 400 °C) peaks for $Ni/CeO_2$ and $Ni/Al_2O_3$ can be due to $H_2$ that is strongly chemisorbed on the catalyst surface. It may also be due to desorption of hydrogen strongly bonded to the substrate of the catalyst or spillovered hydrogen, which would enhance the storage capacity for $H_2$ [35]. Integrated peak areas shown in Table 2 demonstrate that high amounts (242 and 172 μmol/$g_{cat}$ respectively) of total $H_2$ adsorption were exhibited for $Ni/Al_2O_3$ and $Ni/CeO_2$, while only 73 and 61 μmol/$g_{cat}$ for $Ni/TiO_2$ and $Ni/ZrO_2$.

By assuming a stoichiometry ratio of H/Ni = 1, the active surface area, nickel dispersion, and average nickel diameter

**Table 2** Chemisorption results for the reduced Ni-based catalysts with different supports

| Catalyst | $H_2$ uptake (μmol/$g_{cat}$) | $CO_2$ uptake (μmol/$g_{cat}$) | $D_{Ni}$ (%) | $A_{Ni}$ ($m^2$/g-Ni) | $d_{Ni}$ (nm) |
|---|---|---|---|---|---|
| $Ni/Al_2O_3$ | 242 | 24 | 15.0 | 102.7 | 6.6 |
| $Ni/CeO_2$ | 172 | 63 | 10.4 | 71.4 | 9.4 |
| $Ni/TiO_2$ | 73 | 13 | 4.8 | 32.8 | 20.5 |
| $Ni/ZrO_2$ | 61 | 10 | 4.0 | 27.2 | 24.8 |

calculated from the $H_2$-TPD profiles are displayed in Table 2. The dispersion of active sites in the Ni-based catalysts followed an order of $Ni/Al_2O_3 > Ni/CeO_2 > Ni/TiO_2 > Ni/ZrO_2$ and smaller nickel crystallites present in the $Ni/Al_2O_3$ and $Ni/CeO_2$ catalysts, which were in accordance with the results of XRD patterns in Fig. 2b. This is because these two catalysts have larger surface areas and stronger interactions between NiO and support. Furthermore, the strongest interaction between NiO and $Al_2O_3$ resulted in the high dispersion of the metallic Ni on the reduced $Ni/Al_2O_3$ catalyst.

The adsorption of $CO_2$ on the catalyst surface also plays an important role in maintaining the catalytic activity for $CO_2$ methanation and the results are shown in Fig. 4. The profiles of $Ni/ZrO_2$ and $Ni/TiO_2$ exhibited only a small amount of desorbed $CO_2$, while a large amount of desorbed $CO_2$ was detected at 50–300 °C for $Ni/CeO_2$ indicating the existence of weak basic sites. The $CO_2$ desorption was observed in a wide temperature range from 50 °C to 600 °C for $Ni/Al_2O_3$, especially the $CO_2$ desorption peaks at 300–600 °C attributing to the strong basic sites was more remarkable for $Ni/Al_2O_3$ than for the other samples [11]. The amount of $CO_2$ adsorbed was also calculated, referring to the $H_2$ uptake, to be 24, 63, 13 and 10 μmol/$g_{cat}$ for $Ni/Al_2O_3$, $Ni/CeO_2$, $Ni/TiO_2$ and $Ni/ZrO_2$, respectively.

### 3.3 Discussion

To further reveal the structure–activity relationship, the $CO_2$ conversions with $H_2$ and $CO_2$ uptakes at different temperatures over the Ni-based catalysts are co-presented in Fig. 5. Four catalysts all showed low $CO_2$ conversion at 250 °C, because the reaction was controlled by kinetics [36]. With temperature rising to 300 °C, the reaction rate increased and

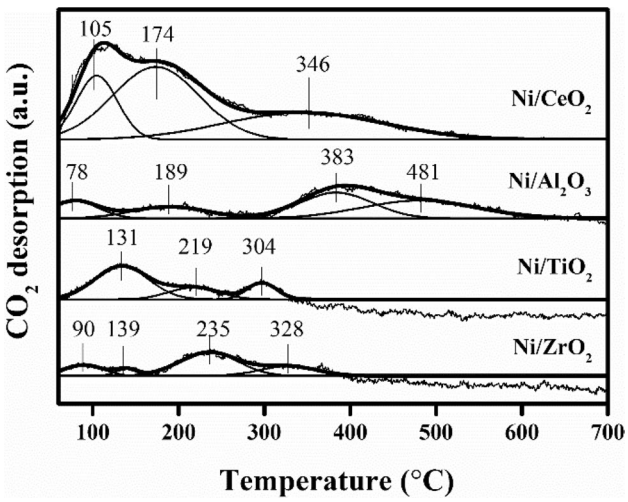


**Fig. 4** $CO_2$-TPD profiles of the Ni-based catalysts with different supports

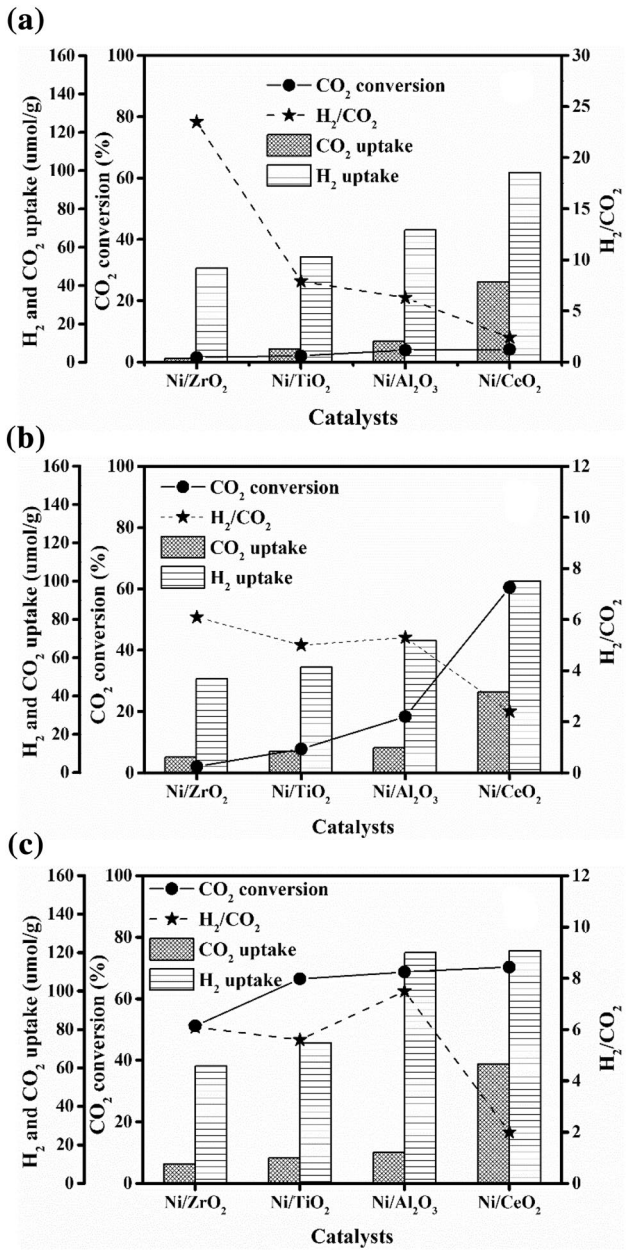


**Fig. 5** Correlation between $CO_2$ conversion and the $H_2$ and $CO_2$ uptakes for the Ni-based catalysts at different temperatures **a** 250 °C **b** 300 °C **c** 400 °C

the adsorbed $H_2$ and $CO_2$ were activated, then $CO_2$ conversion increased over $Ni/CeO_2$ catalyst. For other three catalysts, only 1/3 amount of the $CO_2$ was adsorbed and the $CO_2$ conversions were lower. Elevating the temperature up to 400 °C continuously accelerate the reaction rate and then the $CO_2$ conversion for $Ni/ZrO_2$, $Ni/TiO_2$ and $Ni/Al_2O_3$ catalysts increased rapidly from 10–20% at 300 °C to 50–70% at 400 °C. However, the uptake ratio of $H_2/CO_2$ for $Ni/CeO_2$ was only 2 which is much lower than the stoichiometric factor, which would affect the methanation rate. Stangeland

[29] also reported that high $CO_2$ conversion was difficult to be achieved under 400 °C which was mainly associated with the difficulty of $CO_2$ activation and slow kinetics of methanation.

It is reported [16, 37] that the metal sites on the catalyst adsorb the $H_2$ and provide reactive H-species and the support acts as the active site for $CO_2$ coverage and activation. Therefore, a cooperative catalytic mechanism that enough $H_2$ and $CO_2$ adsorbed on the metallic nickel and support, respectively, followed by subsequent activation and reaction to yield methane, is proposed.

Furthermore, the peak for $CO_2$ desorption from $CeO_2$ lower than 230 °C is assigned essentially to bridged bidentate carbonates species that formed from $CO_2$ absorbed on $Ce^{3+}$ site or oxygen vacancy of the $CeO_2$ surface [38], while the next peak lower than 430 °C is attributed to bidentate and polydentate carbonates on $Ce^{4+}$ support. The highest peak between 430 and 630 °C is assigned to inorganic carboxylate and monodentate carbonate [39]. Therefore, it can be seen from Fig. 4 that $CO_2$ adsorbed on Ni/$CeO_2$ catalyst mainly formed bridged bidentate carbonates species and a part of bidentate or polydentate carbonates because the $CeO_2$ support could be partially reduced to $Ce^{3+}$ by pre-reduction and $H_2$ during reaction. Bridged carbonates site can lower the activation energy for the formation of formate. The dissociated hydrogen on metallic Ni can react with the weakly adsorbed bridged carbonates on the $Ce^{3+}$ site to produce methane and reduced ceria can be oxidized by $CO_2$ at this temperature [40]. The Ni/$CeO_2$ catalyst also provide stronger H adsorption at this temperature, leading to the enhancement of $H_2$ coverage and in the likelihood of hydrogenation of the bridged bidentate carbonates species to $CH_4$.

High temperatures, such as 400 °C, start to be high enough to dissociate $CO_2$ and may tend toward rapid formation of CO then hydrogenate to the formation of methane. Due to the low $H_2$ surface coverage, the selectivity to $CH_4$ was lower than the other three catalysts for Ni/$ZrO_2$ catalyst.

## 4 Conclusions

Four Ni catalysts supported on $Al_2O_3$, $ZrO_2$, $TiO_2$ and $CeO_2$ were prepared and investigated for $CO_2$ methanation performance. The Ni/$CeO_2$ catalyst exhibited the highest $CO_2$ conversion at temperatures lower than 400 °C. The $CO_2$ conversion for the Ni/$CeO_2$ catalyst was 60.1% at 300 °C while that for other three catalysts was all lower than 20%, while the $CH_4$ selectivity all approached to the equilibrium value. The high interaction between nickel and support in the Ni/$Al_2O_3$ catalyst resulted in small metallic nickel well dispersed on the support and the $H_2$ uptake was high as 242 μmol/$g_{cat}$. However, more amount of $CO_2$ was adsorbed on the strong basic sites. Therefore, at low reaction temperatures the $CO_2$ conversion was lower than that over the Ni/$CeO_2$ catalyst, in which Ni nanoparticles and basic support serve as $H_2$ and $CO_2$ active centers respectively and cooperatively catalyze $CO_2$ methanation, resulting in low-temperature reaction activity.

**Acknowledgements** This work was supported by the Fund of State Key Laboratory of Multiphase Complex Systems (No. MPCS-2019-A-04) and International Science and Technology Cooperation Program of China (2018YFE010340).

**Competing interest** There have no competing interest.

## References

1. Zhen W, Gao F, Tian B et al (2017) Enhancing activity for carbon dioxide methanation by encapsulating (111) facet Ni particle in metal–organic frameworks at low temperature. J Catal 348:200–211. https://doi.org/10.1016/j.jcat.2017.02.031
2. Younas M, Loong Kong L, Bashir MJK et al (2016) Recent advancements, fundamental challenges, and opportunities in catalytic methanation of $CO_2$. Energy Fuel 30:8815–8831. https://doi.org/10.1021/acs.energyfuels.6b01723
3. Li W, Zhang A, Jiang X et al (2017) Low temperature $CO_2$ methanation: ZIF-67-derived co-based porous carbon catalysts with controlled crystal morphology and size. ACS Sustain Chem Eng 5:7824–7831. https://doi.org/10.1021/acssuschemeng.7b01306
4. Danaci S, Protasova L, Lefevere J et al (2016) Efficient $CO_2$ methanation over Ni/$Al_2O_3$ coated structured catalysts. Catal Today 273:234–243. https://doi.org/10.1016/j.cattod.2016.04.019
5. Muroyama H, Tsuda Y, Asakoshi T et al (2016) Carbon dioxide methanation over Ni catalysts supported on various metal oxides. J Catal 343:178–184. https://doi.org/10.1016/j.jcat.2016.07.018
6. Beuls A, Swalus C, Jacquemin M et al (2012) Methanation of $CO_2$: further insight into the mechanism over Rh/γ-$Al_2O_3$ catalyst. Appl Catal B Environ 113–114:2–10. https://doi.org/10.1016/j.apcatb.2011.02.033
7. Lin Q, Liu XY, Jiang Y et al (2014) Crystal phase effects on the structure and performance of ruthenium nanoparticles for $CO_2$ hydrogenation. Catal Sci Technol 4:2058–2063. https://doi.org/10.1039/c4cy00030g
8. Karelovic A, Ruiz P (2012) $CO_2$ hydrogenation at low temperature over Rh/γ-$Al_2O_3$ catalysts: effect of the metal particle size on catalytic performances and reaction mechanism. Appl Catal B Environ 113–114:237–249. https://doi.org/10.1016/j.apcatb.2011.11.043
9. Mutz B, Sprenger P, Wang W et al (2018) Operando Raman spectroscopy on $CO_2$ methanation over alumina-supported Ni, $Ni_3Fe$ and $NiRh_{0.1}$ catalysts: role of carbon formation as possible deactivation pathway. Appl Catal A Gen 556:160–171. https://doi.org/10.1016/j.apcata.2018.01.026
10. Xu L, Lian X, Chen M et al (2018) $CO_2$ methanation over Co Ni bimetal-doped ordered mesoporous $Al_2O_3$ catalysts with enhanced low-temperature activities. Int J Hydrog Energy 43:17172–17184. https://doi.org/10.1016/j.ijhydene.2018.07.106
11. Pan Q, Peng J, Sun T et al (2014) Insight into the reaction route of $CO_2$ methanation: promotion effect of medium basic sites. Catal Commun 45:74–78. https://doi.org/10.1016/j.catcom.2013.10.034
12. Ma S, Tan Y, Han Y (2011) Methanation of syngas over coral reef-like Ni/$Al_2O_3$ catalysts. J Nat Gas Chem 20:435–440. https://doi.org/10.1016/s1003-9953(10)60192-2
13. Jia X, Zhang X, Rui N et al (2019) Structural effect of Ni/$ZrO_2$ catalyst on $CO_2$ methanation with enhanced activity. Appl

Catal B Environ 244:159–169. https://doi.org/10.1016/j.apcatb.2018.11.024
14. Tada S, Shimizu T, Kameyama H et al (2012) Ni/$CeO_2$ catalysts with high $CO_2$ methanation activity and high $CH_4$ selectivity at low temperatures. Int J Hydrog Energy 37:527–5531. https://doi.org/10.1016/j.ijhydene.2011.12.122
15. Liu J, Li C, Wang F et al (2013) Enhanced low-temperature activity of $CO_2$ methanation over highly-dispersed Ni/$TiO_2$ catalyst. Catal Sci Technol 3:2627–2633. https://doi.org/10.1039/c3cy00355h
16. He L, Lin Q, Liu Y et al (2014) Unique catalysis of Ni-Al hydrotalcite derived catalyst in $CO_2$ methanation: cooperative effect between Ni nanoparticles and a basic support. Energy Chem 23:587–592. https://doi.org/10.1016/s2095-4956(14)60144-3
17. Vogt C, Groeneveld E, Kamsma G et al (2018) Unravelling structure sensitivity in $CO_2$ hydrogenation over nickel. Nat Catal 1:127–134. https://doi.org/10.1038/s41929-017-0016-y
18. Aldana PAU, Ocampo F, Kobl K et al (2013) Catalytic $CO_2$ valorization into $CH_4$ on Ni-based ceria-zirconia. Reaction mechanism by operando IR spectroscopy. Catal Today 215:201–207. https://doi.org/10.1016/j.cattod.2013.02.019
19. Lin J, Ma C, Wang Q et al (2019) Enhanced low-temperature performance of $CO_2$ methanation over mesoporous Ni/$Al_2O_3$-$ZrO_2$ catalysts. Appl Catal B Environ 243:262–272. https://doi.org/10.1016/j.apcatb.2018.10.059
20. Song F, Zhong Q, Yu Y et al (2017) Obtaining well-dispersed Ni/$Al_2O_3$ catalyst for $CO_2$ methanation with a microwave-assisted method. Int J Hydrog Energy 42:4174–4183. https://doi.org/10.1016/j.ijhydene.2016.10.141
21. Quindimil A, De-La-Torre U, Pereda-Ayo B et al (2018) Ni catalysts with La as promoter supported over Y- and BETA- zeolites for $CO_2$ methanation. Appl Catal B Environ 238:393–403. https://doi.org/10.1016/j.apcatb.2018.07.034
22. Park J-N, McFarland EW (2009) A highly dispersed Pd–Mg/$SiO_2$ catalyst active for methanation of $CO_2$. J Catal 266:92–97. https://doi.org/10.1016/j.jcat.2009.05.018
23. Crespo-Quesada M, Yarulin A, Jin M et al (2011) Structure sensitivity of alkynol hydrogenation on shape- and size-controlled palladium nanocrystals: which sites are most active and selective? J Am Chem Soc 133:12787–12794. https://doi.org/10.1021/ja204557m
24. Hansen TW, Wagner JB, Hansen PL et al (2001) Atomic-resolution in situ transmission electron microscopy of a promoter of a heterogeneous catalyst. Science 294:1508–1510. https://doi.org/10.1126/science.1064399
25. Andersson MP, Abild-Pedersen F, Remediakis IN et al (2008) Structure sensitivity of the methanation reaction: $H_2$-induced CO dissociation on nickel surfaces. J Catal 55:6–19. https://doi.org/10.1016/j.jcat.2007.12.016
26. Wu HC, Chang YC, Wu JH et al (2015) Methanation of $CO_2$ and reverse water gas shift reactions on Ni/$SiO_2$ catalysts: the influence of particle size on selectivity and reaction pathway. Catal Sci Technol 5:4154–4163. https://doi.org/10.1039/c5cy00667h
27. Beierlein D, Schirrmeister S, Traa Y et al (2018) Experimental approach for identifying hotspots in lab-scale fixed-bed reactors exemplified by the Sabatier reaction. React Kinet Mech Catal 125:157–170. https://doi.org/10.1007/s11144-018-1402-4
28. Vita A, Italiano C, Pino L et al (2018) Activity and stability of powder and monolith-coated Ni/GDC catalysts for $CO_2$ methanation. Appl Catal B Environ 226:384–395. https://doi.org/10.1016/j.apcatb.2017.12.078
29. Stangeland K, Kalai DY, Li H et al (2018) Active and stable Ni based catalysts and processes for biogas upgrading: the effect of temperature and initial methane concentration on $CO_2$ methanation. Appl Energy 227:206–212. https://doi.org/10.1016/j.apenergy.2017.08.080
30. Damyanova S, Bueno JMC (2003) Effect of $CeO_2$ loading on the surface and catalytic behaviors of $CeO_2$-$Al_2O_3$-supported Pt catalysts. Appl Catal A Gen 253:135–150. https://doi.org/10.1016/S0926-860X(03)00500-3
31. Du X, Zhang D, Shi L et al (2012) Morphology dependence of catalytic properties of Ni/$CeO_2$ nanostructures for carbon dioxide reforming of methane. Phys Chem C 116:10009–10016. https://doi.org/10.1021/jp300543r
32. Zhang Z, Wei T, Chen G et al (2019) Understanding correlation of the interaction between nickel and alumina with the catalytic behaviors in steam reforming and methanation. Fuel 250:176–193. https://doi.org/10.1016/j.fuel.2019.04.005
33. Cao HX, Zhang J, Ren XK et al (2017) Enhanced CO methanation over Ni-based catalyst using a support with 3D-mesopores. Korean J Chem Eng 34:2374–2382. https://doi.org/10.1007/s11814-017-0148-4
34. Chen S, Miao C, Luo Y et al (2018) Study of catalytic hydrodeoxygenation performance of Ni catalysts: effects of prepared method. Renew Energy 115:1109–1117. https://doi.org/10.1016/j.renene.2017.09.028
35. Li H, Ren J, Qin X et al (2015) Ni/SBA-15 catalysts for CO methanation: effects of V, Ce, and Zr promoters. RSC Adv 5:96504–96517. https://doi.org/10.1039/c5ra15990c
36. Vrijburg W, van Helden J, van Hoof A et al (2019) Tunable colloidal Ni nanoparticles confined and redistributed in mesoporous silica for $CO_2$ methanation. Catal Sci Technol 9:2578–2591. https://doi.org/10.1039/c9cy00532c
37. Liu J, Bing W, Xue X et al (2016) Alkaline-assisted Ni nanocatalysts with largely enhanced low-temperature activity toward $CO_2$ methanation. Catal Sci Technol 6:3976–3983. https://doi.org/10.1039/c5cy02026c
38. Lee S, Lee Y, Moon D et al (2019) Reaction mechanism and catalytic impact of Ni/$CeO_{2-x}$ catalyst for low-temperature $CO_2$ methanation. Ind Eng Chem Res 58:8656–8662. https://doi.org/10.1021/acs.iecr.9b00983
39. Schweke D, Zalkind S, Attia S et al (2018) The interaction of $CO_2$ with $CeO_2$ powder explored by correlating adsorption and thermal desorption analyses. J Phys Chem C 122:9947–9957. https://doi.org/10.1021/acs.jpcc.8b01299
40. Zhou G, Liu H, Cui K et al (2017) Methanation of carbon dioxide over Ni/$CeO_2$ catalysts: effects of support $CeO_2$ structure. Int J Hydrog Energy 42:16108–16117

**Publisher's Note** Springer Nature remains neutral with regard to jurisdictional claims in published maps and institutional affiliations.

## Affiliations

**Yuan Ma[1] · Jiao Liu[2] · Mo Chu[1] · Junrong Yue[2] · Yanbin Cui[2] · Guangwen Xu[3]**

[1] School of Chemical and Environmental Engineering, China University of Mining & Technology (Beijing), Beijing 100083, China

[2] State Key Laboratory of Multi-phase Complex Systems, Institute of Process Engineering, Chinese Academy of Sciences, Beijing 100190, China

[3] Institute of Industrial Chemistry and Energy Technology, Shenyang University of Chemical Technology, Shenyang 110142, Liaoning, China